

**Electrocaloric effects in the lead-free Ba(Zr,Ti)O<sub>3</sub> relaxor ferroelectric from atomistic simulations**Zhijun Jiang,<sup>1,2</sup> Sergei Prokhorenko,<sup>2</sup> Sergey Prosandeev,<sup>2,3</sup> Y. Nahas,<sup>2</sup> D. Wang,<sup>1</sup> Jorge Íñiguez,<sup>4</sup> E. Defay,<sup>4</sup> and L. Bellaiche<sup>2</sup><sup>1</sup>*School of Electronic and Information Engineering & State Key Laboratory for Mechanical Behavior of Materials, Xi'an Jiaotong University, Xi'an 710049, China*<sup>2</sup>*Physics Department and Institute for Nanoscience and Engineering, University of Arkansas, Fayetteville, Arkansas 72701, USA*<sup>3</sup>*Institute of Physics and Physics Department of Southern Federal University, Rostov-na-Donu 344090, Russia*<sup>4</sup>*Materials Research and Technology Department, Luxembourg Institute of Science and Technology, 5 avenue des Hauts-Fourneaux, L-4362 Esch/Alzette, Luxembourg*

(Received 16 April 2017; revised manuscript received 7 June 2017; published 24 July 2017)

Atomistic effective Hamiltonian simulations are used to investigate electrocaloric (EC) effects in the lead-free Ba(Zr<sub>0.5</sub>Ti<sub>0.5</sub>)O<sub>3</sub> (BZT) relaxor ferroelectric. We find that the EC coefficient varies nonmonotonically with the field at any temperature, presenting a maximum that can be traced back to the behavior of BZT's polar nanoregions. We also introduce a simple Landau-based model that reproduces the EC behavior of BZT as a function of field and temperature, and which is directly applicable to other compounds. Finally, we confirm that, for low temperatures (i.e., in nonergodic conditions), the usual indirect approach to measure the EC response provides an estimate that differs quantitatively from a direct evaluation of the field-induced temperature change.

DOI: [10.1103/PhysRevB.96.014114](https://doi.org/10.1103/PhysRevB.96.014114)**I. INTRODUCTION**

The electrocaloric (EC) effect characterizes the change in temperature induced by a change in electric field [1–6], with the electrocaloric coefficient being defined as  $\alpha = \left. \frac{\partial T}{\partial \mathcal{E}} \right|_S$ , where  $T$  is the temperature,  $\mathcal{E}$  is the electric field, and  $S$  is the entropy. It has the potential to be an efficient solid-state refrigeration method for a broad range of applications [6–9]. Numerous studies have been recently conducted via measurements, phenomenologies, and atomistic simulations (see, e.g., Refs. [1,6,10–24], and references therein) and have led to a better knowledge of the electrocaloric effects in typical ferroelectrics, such as BaTiO<sub>3</sub>, LiNbO<sub>3</sub>, Pb(Zr<sub>0.4</sub>Ti<sub>0.6</sub>)O<sub>3</sub>, (Ba<sub>0.5</sub>Sr<sub>0.5</sub>)TiO<sub>3</sub>, as well as antiferroelectrics such as L-doped Pb(Zr,Ti)O<sub>3</sub>. On the other hand, fewer investigations about EC effects have been performed in another class of ferroelectrics, namely, the relaxor ferroelectrics [25–27]. These intriguing materials exhibit unusual features, such as a frequency-dependent and broad dielectric response versus temperature while remaining macroscopically paraelectric down to 0 K [28]. They also display several characteristic temperatures (i.e., the  $T_b$  Burns temperature, the  $T^*$  temperature, and the  $T_m$  temperature) that are associated with a subtle change in some physical properties [29–34]. For instance, in Ba(Zr<sub>0.5</sub>Ti<sub>0.5</sub>)O<sub>3</sub> (BZT) relaxor ferroelectrics, simulations [35] indicate that the Burns temperature (below which the dielectric response does not obey the Curie-Weiss law [36]) is  $T_b \simeq 450$  K,  $T^* \simeq 240$  K, and  $T_m \simeq 130$  K is the temperature at which the dielectric response exhibits a peak, as also in line with measurements in BZT compounds [33,34,37,38]. The microscopic origin of these features is commonly believed to be the existence of so-called polar nanoregions (PNRs) below the Burns temperature [39]. Interestingly, studies devoted to EC effects in relaxor ferroelectrics have resulted in original findings. One example includes the failure of indirect methods (which are based on thermodynamic equilibrium considerations) in the relaxor ferroelectric poly(vinylidene fluoride-trifluoroethylene-chlorofluoroethylene) [P(VDF-TrFE-CFE)] terpolymer to obtain the real change in temperature induced by an electric field for temperatures below which the broad

dielectric constant peaks, because of nonergodicity [25]. Another example is the nonmonotonic behavior of the EC coefficient with the magnitude of the electric field at the fixed critical point temperature  $T_{CP}$  in Pb(Mg,Nb)O<sub>3</sub> (PMN), (Pb,La)(Zr,Ti)O<sub>3</sub>, and Pb(Mg,Nb)O<sub>3</sub>-PbTiO<sub>3</sub> relaxors [27]; especially intriguing is the existence of a maximum of this coefficient at the specific field  $\mathcal{E}_{CP}$  for this  $T_{CP}$  temperature, with  $(T_{CP}, \mathcal{E}_{CP})$  corresponding to the critical point at which the paraelectric-to-ferroelectric transition changes its nature from first order to second order. It is worthwhile to realize that these latter results were obtained for *lead-based* relaxor ferroelectrics while there are also (environmentally friendly) lead-free relaxor ferroelectrics, such as Ba(Zr<sub>1-x</sub>Ti<sub>x</sub>)O<sub>3</sub>, that are fundamentally distinct. For instance, the difference in polarizability between Ti and Zr ions in Ba(Zr<sub>0.5</sub>Ti<sub>0.5</sub>)O<sub>3</sub> was found to be essential to reproduce relaxor behavior via the formation of small Ti-rich PNRs embedded in a paraelectric matrix [35], while the relaxor nature of lead-based PMN was predicted to rather originate from a complex interplay between random electric fields, and ferroelectric and antiferroelectric interactions, yielding much larger PNRs touching each other at low temperatures [40]. Another striking difference between Ba(Zr<sub>0.5</sub>Ti<sub>0.5</sub>)O<sub>3</sub> and PMN is that a recent atomistic simulation did not find any trace of a *first-order* paraelectric-to-ferroelectric phase transition when subjecting Ba(Zr<sub>0.5</sub>Ti<sub>0.5</sub>)O<sub>3</sub> to electric fields, that is, the polarization seems to always continuously evolve with the magnitude of the dc electric field in this lead-free compound [41].

One may therefore wonder about EC effects in lead-free relaxor ferroelectrics, even more when realizing that a recent study done in Ba(Zr<sub>1-x</sub>Ti<sub>x</sub>)O<sub>3</sub> with  $x = 0.20$  reported a giant  $\alpha$  electrocaloric coefficient [42,43] [note that this system is different from Ba(Zr<sub>0.5</sub>Ti<sub>0.5</sub>)O<sub>3</sub> in the sense that it possesses a polar ground state in addition to some relaxor features]. For instance, many questions remain to be addressed in Ba(Zr<sub>0.5</sub>Ti<sub>0.5</sub>)O<sub>3</sub>: Do indirect and direct methods also provide different results below a specific temperature? How does  $\alpha$  behave with the dc electric field for the different temperature ranges in BZT, i.e., above  $T_b$ , between  $T_b$  and  $T^*$ , between  $T^*$

and  $T_m$ , and below  $T_m$ ? In particular, can  $\alpha$  exhibit a maximum for some intermediate field at any of these temperature ranges? If such a maximum exists, what is its microscopic origin? Other natural questions to ask are if and how  $\alpha$  depends on temperature for fixed electric fields, and if it is possible to reproduce and understand such a (presently unknown) dependency.

As we will see below, this article provides an answer to all these open questions, by conducting and analyzing atomistic simulations on Ba(Zr<sub>0.5</sub>Ti<sub>0.5</sub>)O<sub>3</sub> ferroelectric relaxors. This article is organized as follows. Section II provides details about the methods used here. Results are given, analyzed, and explained in Sec. III. Finally, Sec. IV concludes this work.

## II. METHODS

We use here a first-principles-based effective Hamiltonian ( $H_{\text{eff}}$ ) approach that has been recently developed for Ba(Zr<sub>0.5</sub>Ti<sub>0.5</sub>)O<sub>3</sub> (BZT) solid solutions [35,41,44–46]. The total energy of the effective Hamiltonian used here contains two main terms,  $E_{\text{int}}(\{\mathbf{u}_i\}, \{\mathbf{v}_i\}, \eta_H, \{\sigma_j\}) = E_{\text{ave}}(\{\mathbf{u}_i\}, \{\mathbf{v}_i\}, \eta_H) + E_{\text{loc}}(\{\mathbf{u}_i\}, \{\mathbf{v}_i\}, \{\sigma_j\})$ , where  $\mathbf{u}_i$  is the local soft mode in unit cell  $i$  (which is related to the electric dipole of that cell and that is technically centered on the Zr or Ti ions),  $\mathbf{v}_i$  are variables related to the inhomogeneous strain inside each cell,  $\eta_H$  is the homogeneous strain tensor, and  $\{\sigma_j\}$  represents the atomic configuration of the BZT solid solutions (i.e., how Zr and Ti ions are distributed within the  $B$  sublattice of BZT).  $E_{\text{ave}}$  contains five energetic terms: (i) the local-mode self-energy; (ii) the long-range dipole-dipole interaction; (iii) the energy due to short-range interactions between local modes; (iv) the elastic energy; and (v) the energy representing the interaction between local modes and strains [47].  $E_{\text{loc}}$  describes how the actual distribution of Zr and Ti cations affects the energetics involving the local soft modes  $\mathbf{u}_i$  and the local strain variables, and therefore depends on the  $\{\sigma_j\}$  distribution [35,41,44]. One can also add to  $E_{\text{int}}$  an energy that is proportional to the dot product between polarization and electric field, in order to mimic the effect of such a field on physical properties.

This effective Hamiltonian successfully predicted the existence of three characteristic temperatures in BZT, namely, the Burns temperature ( $T_b \simeq 450$  K), below which the dielectric response no longer follows the Curie-Weiss law [36], the so-called  $T^*$  (that is close to  $\simeq 240$  K), and the  $T_m$  temperature at which the dielectric response can exhibit a peak ( $T_m \simeq 130$  K) [35], as consistent with experimental findings for BZT systems [33,34,37,38]. This atomistic scheme also yields polar nanoregions inside which the Ti-centered dipoles are aligned parallel to each other, with these PNRs being dynamic in nature between  $T^*$  and  $T_b$ , while, below  $T_m$ , they are static and all have a polarization pointing along one of the eight (111) pseudocubic directions [35]. The polarizations of these different PNRs cancel each other, as consistent with the fact that BZT is macroscopically paraelectric down to 0 K [33–35,37,38]. This effective Hamiltonian was also successful in reproducing the unusual dielectric relaxation known to occur in relaxor ferroelectrics [46]. Here, we implement this  $H_{\text{eff}}$  within Monte Carlo (MC) and molecular dynamics (MD) simulations, in order to determine and understand EC effects in BZT relaxors, as modeled by  $14 \times 14 \times 14$  supercells (13 720 atoms) in the

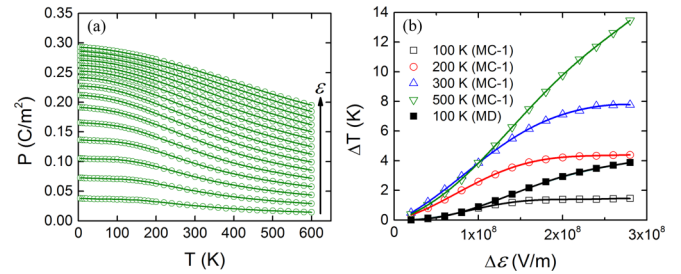


FIG. 1. Physical properties associated with the MC-1 method. (a) shows the temperature dependency of the polarization in BZT systems subject to different dc electric fields, all applied along the pseudocubic [001] direction but varying from  $2.0 \times 10^7$  to  $3.0 \times 10^8$  V/m in magnitude in steps of  $2.0 \times 10^7$  V/m. (b) shows the resulting change in temperature as a function of  $\Delta\mathcal{E} = \mathcal{E}_2 - \mathcal{E}_1$  for four selected initial temperatures, as computed from Eq. (1) and choosing  $\mathcal{E}_1 = 2.0 \times 10^7$  V/m. Note that (b) also further reports the direct change in temperature at 100 K as a function of  $\mathcal{E}_f$ .

MC computations and  $32 \times 32 \times 32$  (32 768 atoms) in the MD simulations. Note that this different choice of supercells between the MC and MD simulations originates from the fact that the code we used for the MD computations can handle larger supercells, and that the use of  $32 \times 32 \times 32$  supercells allows the temperature change in MD simulations to be easily sorted out from the temperature fluctuations. Note also that we numerically checked that the use of  $12 \times 12 \times 12$ ,  $14 \times 14 \times 14$ , and  $16 \times 16 \times 16$  supercells provides similar results, which suggests that our Monte Carlo simulations are free from significant size effects. These supercells are periodic along the three Cartesian directions, and Zr and Ti atoms are randomly distributed inside them. We also average our physical results over 20 random configurations for both MC and MD simulations, in order to mimic well disordered BZT solid solutions.

Let us now indicate how we practically compute, from these simulations, the electrocaloric coefficient  $\alpha = \left. \frac{\partial T}{\partial \mathcal{E}} \right|_S$ . One approach we use here is based on the Maxwell thermodynamic relationship  $\left. \frac{\partial S}{\partial \mathcal{E}} \right|_T = \left. \frac{\partial P}{\partial T} \right|_{\mathcal{E}}$  leading to the adiabatic temperature change,

$$\Delta T = - \int_{\mathcal{E}_1}^{\mathcal{E}_2} \frac{T(\mathcal{E})}{C_{\mathcal{E}}(T)} \left. \frac{\partial P}{\partial T} \right|_{\mathcal{E}} d\mathcal{E}, \quad (1)$$

where  $P$  is the macroscopic polarization and  $C_{\mathcal{E}}$  is the heat capacity per unit volume under constant dc electric field. Such a latter equation therefore tells us that we can obtain  $\alpha$  from MC simulations by computing

$$\alpha = - \left. \frac{T}{C_{\mathcal{E}}} \frac{\partial P}{\partial T} \right|_{\mathcal{E}}. \quad (2)$$

This way of extracting  $\alpha$  is coined MC-1 here.

For instance, Fig. 1(a) reports the polarization as a function of temperature obtained from MC simulations on Ba(Zr<sub>0.5</sub>Ti<sub>0.5</sub>)O<sub>3</sub>, for dc electric fields all applied along the pseudocubic [001] direction and ranging between  $2.0 \times 10^7$  and  $3.0 \times 10^8$  V/m in magnitude. Values of  $\left. \frac{\partial P}{\partial T} \right|_{\mathcal{E}}$  are then obtained from cubic  $B$ -spline fits to these  $P(T)$  curves, which allow us to determine  $\alpha$  via Eq. (2). Note that the heat capacity at a given electric field  $\mathcal{E}$  is calculated as

$C_{\mathcal{E}} = (N \frac{\langle E_{\text{int}}^2 \rangle - \langle E_{\text{int}} \rangle^2}{T^2 k_B} + \frac{15}{2} k_B) / V$ , where  $N$  is the number of sites in the supercell,  $E_{\text{int}}$  is the total internal energy provided by the effective Hamiltonian,  $\langle \rangle$  denotes the average over the MC sweeps at every considered  $T$  temperature,  $k_B$  is the Boltzmann constant, and  $V$  is the volume of the primitive unit cell. The factor  $\frac{15}{2}$  in that formula reflects that there are five atoms in the unit cell of perovskites [16]. Moreover,  $C_{\mathcal{E}}$  is computed for different temperatures and electric fields, implying that it can, in principle, depend on  $T$  and  $\mathcal{E}$ . However, we numerically found that these dependencies are rather weak, as consistent with measurements [42], and that  $C_{\mathcal{E}}$  is always very close to  $2.18 \text{ MJ/K m}^3$ .

Interestingly, there is another way to obtain the EC coefficient from MC runs, that is, by taking advantage of the cumulant formula given in Ref. [48],

$$\alpha = -Z^* a_{\text{lat}} N T \left\{ \frac{\langle |\mathbf{u}| E_{\text{int}} \rangle - \langle |\mathbf{u}| \rangle \langle E_{\text{int}} \rangle}{\langle E_{\text{int}}^2 \rangle - \langle E_{\text{int}} \rangle^2} \right\}, \quad (3)$$

where  $Z^*$  is the Born effective charge,  $a_{\text{lat}}$  is the five-atom lattice constant,  $N$  is the number of sites in the supercell,  $T$  is the considered temperature,  $\mathbf{u}$  is the supercell average of the local mode,  $E_{\text{int}}$  is the total energy of the effective Hamiltonian, and  $\langle \rangle$  denotes the average over the MC sweeps at every considered temperature. This method will be called MC-2 here. Technically, the computation of  $\alpha$  via Eq. (3) is done for a chosen combination of temperature and magnitude of a dc electric field applied along the pseudocubic [001] direction, which therefore allows us to determine the effect of temperature and applied electric field on the EC coefficient. In the following, we will also be interested in comparing the predictions of MC-1 and MC-2, mostly because the MC-2 method is less known than MC-1 while being computationally more accurate (since, unlike MC-1, it does not rely on a fit of  $\frac{\partial P}{\partial T} |_{\mathcal{E}}$ ).

Regarding the direct approach, we determine the electrocaloric coefficient by using the ramping method of Ref. [18] within molecular dynamics. First, an Evans-Hoover thermostat [49,50] is used in the MD simulations in order to equilibrate the system at an initial temperature  $T$  when no electric field is applied. The electric field is then applied along the pseudocubic [001] direction and ramped up (with time) from zero to a specific value,  $\mathcal{E}_f$ , and then ramped down from  $\mathcal{E}_f$  to zero. Practically, we chose the time dependence of the applied field  $\mathcal{E}(t)$  amplitude to be

$$\mathcal{E}(t) = \frac{\mathcal{E}_f}{2} \left[ \tanh \left( \frac{t - t_{\text{up}}}{\tau} \right) - \tanh \left( \frac{t - t_{\text{down}}}{\tau} \right) \right], \quad (4)$$

where  $t_{\text{up}}$  and  $t_{\text{down}}$  denote the times when the field magnitude reaches  $\mathcal{E}_f/2$  during ramping up and down, respectively. The ramping up/down time frames thus correspond to

$$t_{\text{up/down}} - \tau/2 \lesssim t \lesssim t_{\text{up/down}} + \tau/2, \quad (5)$$

with  $\tau$  representing the time interval during which the field on/off switching happens. The ‘‘hyperbolic tangent’’ time profile is commonly used in linear response calculations and was chosen to obtain a smooth time dependence of the external field. Notably, we observed no significant differences with test calculations where the time dependence of the external field was assumed linear, as described in Ref. [18]. To test the

convergence of results with respect to  $\tau$ , and the integration time step  $\Delta t$ , the test runs were performed for values of  $\tau$  ranging from 20 to 200 ps and values of  $\Delta t$  from 0.001 to 4 fs. All the simulations were performed using the Omelyan second-order symplectic integration algorithm [51]. Based on the convergence tests, the final chosen value of  $\tau$  was of 188 ps with  $\Delta t$  equal to 0.1 fs, ensuring the energy conservation for a constant field simulation up to a maximum relative error of  $10^{-6}$ . The inverse rate of the change of the applied field was thus close to 188 fs cm/kV for an applied field magnitude of 1000 kV/cm. For the chosen simulation parameters, we find that the calculated field-induced temperature change upon ramping down  $\Delta T_{\text{down}}$  is equal in magnitude, but opposite in sign, to the temperature change  $\Delta T_{\text{up}}$  produced by the switching on the external field for temperatures above  $T_m$ , a result that is naturally expected for time-reversible processes. However, for  $T < T_m$ , during the ramping down of the applied field, the temperature first exhibited a drop, which was subsequently followed by an increase (note that this result was also tested for convergence with respect to  $\tau$  and  $\Delta t$ ). Such behavior, broadly speaking, can be attributed to the loss of ergodicity below  $T_m$ . A detailed investigation of the microscopic mechanism responsible for this unusual behavior lies beyond the scope of the current study and, for the purposes of the present work, the EC temperature change  $\Delta T$  was defined to be equal to  $\Delta T_{\text{up}}$ , and the  $\alpha$  EC coefficient associated with a specific field’s magnitude can then be obtained by taking the derivative of  $\Delta T_{\text{up}}$  with respect to  $\mathcal{E}_f$  at this specific field’s magnitude. Such results will be denoted as ‘‘MD’’ here [52].

Note that data from MC-1 and MC-2 approaches can be considered to be associated with the *indirect method* to obtain EC effects, because they are based on thermodynamic equilibrium. On the other hand, data obtained from MD computations yield the *direct* EC effects, which may differ from those obtained from the indirect way for systems adopting nonergodic behavior, as the one that relaxors are known to exhibit below some specific temperature  $T_m$  at which the dielectric response peaks [53]. Comparisons between our MC and MD results should thus tell us the difference between the indirect and direct ways to extract EC effects in relaxors. Since we are also interested in checking if and how this difference (if any) depends on the investigated temperature region, we decided to focus on four particular representative temperatures. They are (1) 500 K, which is above the predicted Burns temperature ( $T_b \simeq 450 \text{ K}$ ) of BZT [35,37], (2) 300 K, which is located in between our critical  $T^* \simeq 240 \text{ K}$  [33–35] and  $T_b$ , (3) 200 K, that is now between the computed  $T_m$  temperature of BZT ( $T_m \simeq 130 \text{ K}$ ) [35,38] and  $T^*$ , and (4) 100 K, which is thus below  $T_m$  (note that the Supplemental Material [54] also shows our results for the EC coefficient in BZT at 600 K).

### III. RESULTS

#### A. EC coefficients

Figure 2 shows the electrocaloric coefficient as a function of electric field  $\mathcal{E}$  for these four different selected temperatures, and as computed from the aforementioned MC-1, MC-2, and MD methods. One can first clearly see that, for any of

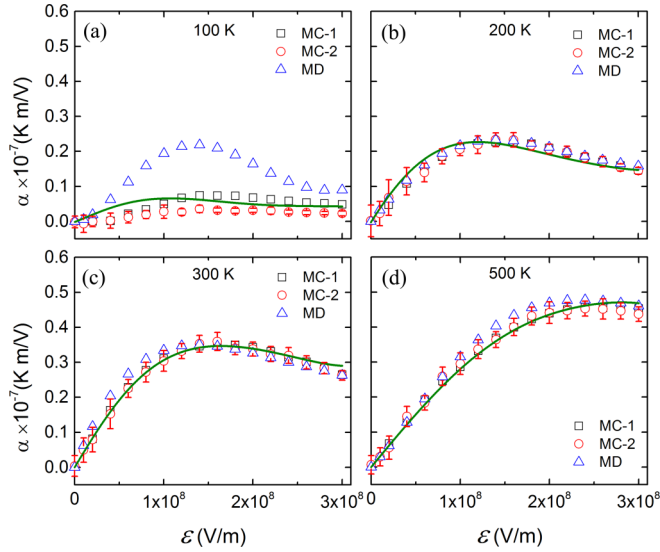


FIG. 2. Electrocaloric coefficient  $\alpha$  as a function of the applied dc electric field  $\mathcal{E}$ , as predicted for the different indirect and direct approaches at (a) 100, (b) 200, (c) 300, and (d) 500 K. The solid green line represent the fit of the MC-1 and MC-2 results by the second line of Eq. (9), i.e.,  $\alpha = \beta T \frac{\partial P^2}{\partial \mathcal{E}}|_T$ , where  $\beta$  is a constant and  $\frac{\partial P^2}{\partial \mathcal{E}}|_T$  is obtained from the data of Fig. 3. Error bars (resulting from the use of 20 different disordered alloy configurations) are also shown for the MC-2 data.

these temperatures, the (indirect) MC-1 and MC-2 approaches provide nearly identical results. Similarly,  $\alpha$  predicted by the (direct) MD scheme agrees very well with those of MC-1 and MC-2 for 200, 300, and 500 K at any field, which demonstrates that indirect methods based on Maxwell's thermodynamic relation can be safely used to estimate  $\alpha$  above the  $T_m$  temperature of relaxors. On the other hand, Fig. 2(a) clearly reveals that the EC coefficient of the MD method significantly differs from that predicted by MC-1 and MC-2 at 100 K, as a result of nonergodicity. In particular, at 100 K, the  $\alpha$  deduced from the indirect methods are smaller than that those directly extracted, which is in agreement with previous reports [25,53,60]. It is also interesting to realize that the EC coefficient of the MD method gets closer to those of MC-1 and MC-2 at 100 K for the highest considered electric fields. This is because, under high electric fields, BZT relaxors can be converted to a normal ferroelectric and thus become ergodic [41].

Moreover, the results of Fig. 2(d) also indicate that  $\alpha$  at 500 K is vanishing at small fields and then increases with  $\mathcal{E}$ , until it very slightly decreases for our highest investigated fields. Interestingly, our values of  $\alpha$  for high fields at 500 K are of the order of  $0.5 \times 10^{-7}$  K m/V, which is similar to the predicted one of  $0.67 \times 10^{-7}$  K m/V in a ferroelectric phase of (Ba,Sr)TiO<sub>3</sub> [15]. Figures 2(a)–2(c) also show that, for temperatures below the Burns temperature,  $\alpha$  adopts a very clear *maximum* for an intermediate field (whose value is dependent on temperature) within our investigated range of electric fields. In other words, at temperatures of 300, 200, or 100 K, the EC coefficient first increases with field before noticeably decreasing. Such nonmonotonic behavior of  $\alpha$  (starting with a vanishing value at small fields and

having a peak for an intermediate field before decreasing for larger fields) was indeed measured, as well as reproduced by the so-called phenomenological spherical random bond random field model, in Pb(Mg,Nb)O<sub>3</sub>, (Pb,La)(Zr,Ti)O<sub>3</sub>, and Pb(Mg,Nb)O<sub>3</sub>-PbTiO<sub>3</sub> relaxors in Ref. [27], but only for a specific temperature: namely, the critical temperature at which the discontinuous electric-field-induced ferroelectric transition of these systems becomes continuous (for the value of the electric field associated with the maximum of  $\alpha$ ). Our results displayed in Fig. 2 therefore generalize such findings by indicating that, for *any* temperature,  $\alpha$  of BZT can also exhibit a maximum within the investigated field range. Further, note also that BZT differs from the cases of Pb(Mg,Nb)O<sub>3</sub>, (Pb,La)(Zr,Ti)O<sub>3</sub>, and Pb(Mg,Nb)O<sub>3</sub>-PbTiO<sub>3</sub> in the sense that the temperature behavior of the polarization displayed in Fig. 1(a) is always continuous for any investigated field. It is worthwhile to know that the maximum of  $\alpha$  at a certain field was also predicted to occur in Ba<sub>0.5</sub>Sr<sub>0.5</sub>TiO<sub>3</sub> [16] and defect-doped BaTiO<sub>3</sub> [61], and that we also found this nonmonotonic behavior of  $\alpha$  in the paraelectric phase of BaTiO<sub>3</sub> (BTO) bulk, as evidenced in the Supplemental Material [54].

## B. Analysis of the results via a Landau-like model

Let us now try to understand the main results of Fig. 2. For that, we start from a simplest Landau free-energy potential describing the behavior of a nonlinear dielectric,

$$\begin{aligned} F &= F_0(T) + \Delta F(T, P, \mathcal{E}) \\ &= F_0(T) + \frac{1}{2}a(T)P^2 + \frac{1}{4}bP^4 - \mathcal{E}P, \end{aligned} \quad (6)$$

where  $F_0(T)$  captures the basic temperature dependence of the free energy of the materials, and the other terms account for the variations that involve the development of a polarization or application of an electric field. Note that the temperature dependence of the harmonic  $a(T)$  parameter can be a complex one in our BZT compound with various regimes, as inferred from the temperature behavior of the dielectric response under the dc field and discussed in Ref. [35]: For  $T > T_b$  we have  $a(T) \propto (T - T_0)$ , while for  $T < T_m$  we have  $da(T)/dT \sim 0$ , and for  $T_m < T < T_b$  we have a smooth interpolation between these two regimes [note that (i)  $T_0$  is extracted from the Curie-Weiss behavior of the dielectric response above  $T_b$  and can be negative in relaxor ferroelectrics, as predicted and experimentally found in Refs. [35,37], and (ii) that the aforementioned behaviors of  $a(T)$  imply that it is increasing with temperature above  $T_m$ ]. In the following equations we will work with a generic  $a(T) > 0$ , noting that the final results have to be interpreted depending on the  $T$  region we are in. In particular, the phenomenological equations to be derived here [namely, Eqs. (6)–(16)] can only be safely applied to temperatures above  $T_m$ . This is because these equations rely on thermodynamic equilibrium while BZT is nonergodic below  $T_m$ . Finally, the positive parameter  $b > 0$  accounts for the saturation of the dielectric response of the material.

Let us now discuss the behavior of the EC coefficient as predicted by this simple model. The entropy can be obtained as

$$S = -\frac{dF}{dT} = -\frac{dF_0}{dT} - \frac{\partial \Delta F}{\partial T} - \frac{\partial \Delta F}{\partial P} \frac{dP}{dT}. \quad (7)$$

Noting that at equilibrium we have  $\partial \Delta F / \partial P = 0$ , we obtain

$$S = -\frac{dF_0}{dT} - \frac{a'(T)}{2} P^2, \quad (8)$$

where  $a' = da/dT$ . It is then straightforward to derive the following expression for  $\alpha$ ,

$$\begin{aligned} \alpha &= -\left. \frac{T}{C_{\mathcal{E}}} \frac{\partial S}{\partial \mathcal{E}} \right|_T \\ &= \left. \frac{T a'(T)}{2 C_{\mathcal{E}}} \frac{\partial P^2}{\partial \mathcal{E}} \right|_T \\ &= \frac{T a'(T)}{C_{\mathcal{E}}} P \chi, \end{aligned} \quad (9)$$

where  $\chi$  is the dielectric susceptibility.

Interestingly, the behavior of a dielectric for small electric fields can be readily discussed from this expression. Indeed, if  $P = 0$  for  $\mathcal{E} = 0$ , then we have  $P = \chi \mathcal{E}$ , which leads to  $\alpha \propto \mathcal{E}$ , assuming that the dependence of the specific heat  $C_{\mathcal{E}}$  on the electric field can be neglected. This prediction is fully consistent with the null value of  $\alpha$  reported in Fig. 2 at zero field for any temperature, and immediately implies that  $\Delta T \propto \mathcal{E}^2$ , which shows that the EC effect is null in the limit of small  $\mathcal{E}$ .

To discuss the behavior of  $\alpha$  for arbitrary electric field values, we recall the equilibrium condition  $\partial F / \partial P = 0$  to obtain

$$a(T)P + bP^3 = \mathcal{E}. \quad (10)$$

Further, if we take the derivative with respect to the electric field on both sides of this equation, we get

$$a(T)\chi + 3bP^2\chi = 1, \quad (11)$$

which leads to

$$\alpha = \frac{2T}{C_{\mathcal{E}}} \frac{a'(T)P}{a(T) + 3bP^2}. \quad (12)$$

This interesting expression implies that, in the limit of large polarizations (or, equivalently, large electric fields), we have  $\alpha \rightarrow 0$ . Hence, since we also know that  $\alpha = 0$  for  $\mathcal{E} = P = 0$ , it immediately follows that the EC coefficient will present at least one extremum (maximum or minimum) at intermediate values of the electric field, as also consistent with our numerical results of Fig. 2. Of course, whether or not such an extremum is experimentally accessible will depend on the breakdown field of a particular material or sample; yet, at least one extremum has to exist in principle. Note also that  $\alpha$  will adopt a maximum if  $a'(T)$  is positive (which is the case of BZT) while it will possess a minimum if  $a'(T)$  is negative.

To find the electric field that makes  $\alpha$  maximum, we have to solve

$$\frac{d\alpha}{d\mathcal{E}} = -\frac{2a'(T)}{C_{\mathcal{E}}} (\chi^2 + P_m \chi') = 0, \quad (13)$$

where  $\chi' = d\chi/d\mathcal{E}$  captures the nonlinear dielectric response of the material, and  $P_m$  is the value of the polarization for which  $\alpha$  is maximum. The nonlinear response  $\chi'$  is related to  $P$  and  $\chi$  by

$$a(T)\chi' + 6bP\chi^2 + 3bP^2\chi' = 0, \quad (14)$$

which we obtain by taking the field derivative of both sides of Eq. (11). From the last two relations, one can show that the condition to have an extremum of  $\alpha$  reduces to

$$P_m^2 = \frac{a(T)}{3b}, \quad (15)$$

from which several conclusions can be immediately drawn. First, for stiff materials, i.e., those with  $a(T) \gg 0$ , the extremum of  $\alpha$  will occur at relatively large value of the polarization and applied electric field. Similarly, if the dielectric response is very linear, i.e., for small  $b > 0$ , the extremum of  $\alpha$  will also tend to occur for large values of  $P$  and  $\mathcal{E}$ . Finally, using a linear approximation for the polarization as a function of field,  $P \sim \chi \mathcal{E}$ , we can write

$$\mathcal{E}_m^2 \approx \frac{a(T)}{3b\chi^2} = \frac{4a^3(T)}{3b}, \quad (16)$$

which provides us with a useful (albeit approximate) expression for the electric field corresponding to  $\alpha$ 's extremum. For instance, it tells us that  $\mathcal{E}_m$  should increase with temperature if  $a(T)$  is enhanced with temperature (which is precisely the case for BZT). This increase of  $\mathcal{E}_m$  with temperature is indeed confirmed in Fig. 2 for temperatures above 200 K, and is also consistent with the fact that, at 500 K, the maximum of  $\alpha$  occurs for electric fields being close to our highest investigated values.

Moreover, the second line of Eq. (9) indicates that  $\alpha = \beta T \left. \frac{\partial P^2}{\partial \mathcal{E}} \right|_T$ , with  $\beta = \frac{a'(T)}{2C_{\mathcal{E}}}$ . In other words, assuming that  $C_{\mathcal{E}}$  is independent of temperature and electric field, and that  $a'(T)$  is also a constant (which is, e.g., what Curie-Weiss law [36] provides), this expression implies that the numerical data of the MC-1 and MC-2 approaches for the EC coefficient should be well fitted by the product of temperature and the derivative of the square of the polarization with respect to electric field, once rescaling this product by a constant [62,63]. Figure 2 indeed tells us that this is the case for any temperature (especially at and above 200 K, where we are in ergodic equilibrium conditions), since these figures further display the results of such fits by means of solid green curves. In other words, one can safely use Eq. (9) to reproduce and understand the EC coefficients numerically obtained by the indirect methods for any temperature and field [note that the Supplemental Material also shows that Eq. (9) can be accurately used for the  $\alpha$  coefficient of typical ferroelectrics, such as BaTiO<sub>3</sub>, which further emphasizes its generality]. In particular, the second line of Eq. (9) indicates that, for a given temperature, the nonmonotonic and unusual behavior of  $\alpha$  with fields obtained by MC-1 and MC-2 should be directly related to the dependence of  $\left. \frac{\partial P^2}{\partial \mathcal{E}} \right|_T$  with  $\mathcal{E}$ . To check such an interesting idea, Figs. 3(a)–3(d) report the square of the macroscopic polarization as a function of electric field applied along the [001] direction at 100, 200, 300, and 500 K, respectively. The central inset of these figures displays the derivative of this quantity with respect to the field, and reveals that, indeed,  $\left. \frac{\partial P^2}{\partial \mathcal{E}} \right|_T$  has the same trend as the indirect EC coefficient of Fig. 2. In particular, Figs. 3(a)–3(d) reveal that  $\alpha$  is very small for low fields at any temperature, simply because the square of the polarization is basically independent of electric fields for small  $\mathcal{E}$  [64]. Such a strong connection between  $\alpha$

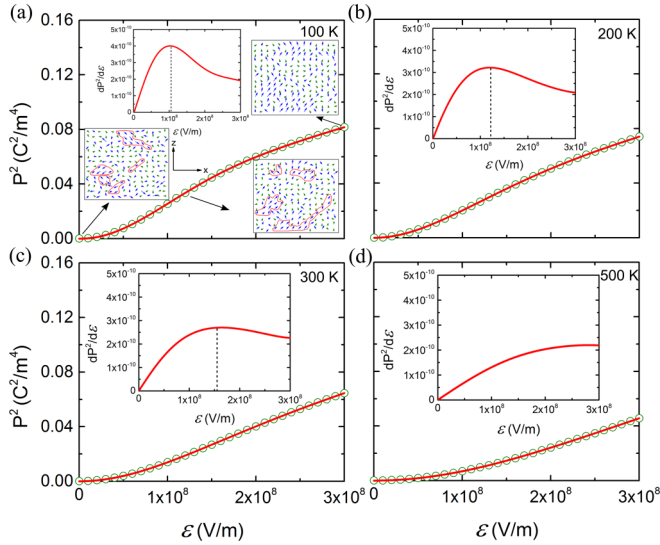


FIG. 3. The square of the macroscopic polarization as a function of the applied dc electric field, at (a) 100, (b) 200, (c) 300, and (d) 500 K. The red line represents a fit by seventh degree polynomials, which were then used to calculate the derivative  $dP^2/dE$  that is shown in the corresponding central inset of each panel. The other insets of (a) show the dipolar configurations in a given  $(x, z)$  plane at 100 K, as obtained from MC simulations for different dc electric fields ( $0$ ,  $1.2 \times 10^8$ , and  $3.0 \times 10^8$  V/m) applied along the pseudocubic [001] direction. In these latter insets, the blue and green colors indicate that the local dipoles are centered on Ti and Zr ions, respectively, and the red solid lines delimit the PNRs.

and  $\frac{\partial P^2}{\partial E}|_T$  is reinforced when realizing that the field resulting in a maximum of the  $\alpha$  coefficient of the MC-1 and MC-2 methods at 100, 200, 300, and 500 K is very close to the field at which  $\frac{\partial P^2}{\partial E}|_T$  is optimal at these temperatures. It is also interesting to realize that the maximal value of the  $\alpha$  of the indirect methods increases by a factor of about 3 when increasing the temperature from 100 to 300 K, while the corresponding maximum of  $\frac{\partial P^2}{\partial E}|_T$  is quite similar between 100 and 300 K. Such a feature can, in fact, be understood by the fact that the second line of Eq. (9) indicates that the EC coefficient is directly proportional to the temperature. In other words, increasing the temperature increases  $\alpha$  in the case of similar  $\frac{\partial P^2}{\partial E}|_T$  (note that Eq. (9) is also consistent with the computational finding of the enhancement of  $\alpha$  with temperature in the ferroelectric phases of (Ba,Sr)TiO<sub>3</sub> in Ref. [15]).

### C. Microscopic insights

Let us now try to reveal the *microscopic* origins of the maximum of  $\frac{\partial P^2}{\partial E}|_T$  at 200 and 300 K (which explains the maximum of the indirect and direct  $\alpha$  of these temperatures) as well as the peak of the  $\alpha$  obtained by the MD simulations at 100 K [recall that, for temperatures below  $\approx 130$  K, BZT is nonergodic and thus cannot be technically described by Eq. (9)]. For that, we focus on the field evolution of the microscopic configurations of BZT at 100 K. Some insets of Fig. 3(a) show dipolar snapshots within a given  $(x, z)$  plane obtained from MC simulations at 100 K for different electric

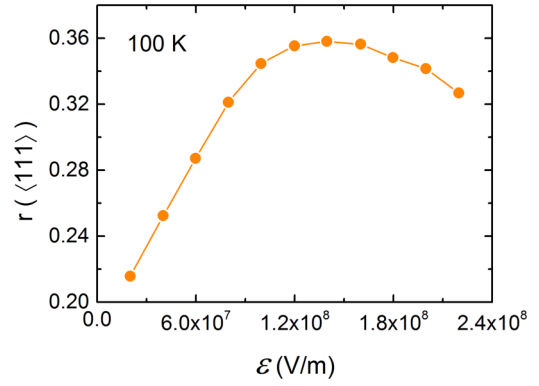


FIG. 4. The ratio of dipoles that are pointing along  $\langle 111 \rangle$  directions having a positive  $z$  component, as a function of the magnitude of the electric field applied along the pseudocubic [001] direction at 100 K. Note that these  $\langle 111 \rangle$  directions are thus away from the [001] field's direction.

fields. They reveal that the microscopic dipolar pattern is rather complex and sensitive to electric fields. For instance, there are different polar nanoregions inside which the dipoles centered on Ti ions align along one of the eight  $\langle 111 \rangle$  pseudocubic directions (with this direction varying from one PNR to another, e.g., from  $[111]$  to  $[11\bar{1}]$ ), when no external field is applied [see the left bottom inset of Fig. 3(a)]. Increasing the electric field then leads to the local dipoles of the PNRs rotating towards the field's direction, as well as the formation of rather large PNRs having local dipoles lying along the applied electric field direction [see the bottom right inset of Fig. 3(a) for a field of  $1.2 \times 10^8$  V/m]. Finally, Fig. 3(a) further indicates that increasing the field up to our considered maximum value  $E = 3.0 \times 10^8$  V/m causes nearly all Ti-centered local dipoles to align along the field's direction, which can be seen as indicative that BZT is converting from a relaxor behavior to a normal ferroelectric [see the top right inset of Fig. 3(a)].

Interestingly, the aforementioned field-induced rearrangement of the local dipoles for fields close to  $1.2 \times 10^8$  V/m generates a maximal change of the entropy, as evidenced by the fact that Fig. 4 reveals that the fields associated with maximal values of  $\alpha$  obtained by the direct approach at 100 K [see Fig. 2(a)] are precisely the fields for which a specific microscopic feature occurs: The number of dipoles pointing along  $\langle 111 \rangle$  pseudocubic directions for which the  $z$  component is positive (i.e., which have a  $z$  component parallel to the applied electric field) is maximal for these fields. This microscopic feature was also numerically found (not shown here) for the fields associated with the maximum values of  $\alpha$  at 200 and 300 K (note that BZT does not possess any PNR at 500 K because this latter temperature is above the Burns temperature).

### D. Resulting change in temperature

Let us now concentrate on the  $\Delta T$  change in temperature, associated with the EC coefficient and as computed from Eq. (1), for the four studied temperatures of 100, 200, 300, and 500 K. Note that, unlike for 200, 300, and 500 K, this change in temperature will not be the “direct” one for 100 K because the system is nonergodic at this temperature, while

Eq. (1) assumes thermodynamic equilibrium. We nevertheless report in Fig. 1(b) the data for  $\Delta T$  as a function of a change in electric field  $\Delta \mathcal{E}$  at 100 K, along with those of 200, 300, and 500 K, for the sake of comparison. Technically, the  $\Delta T$  of Eq. (1) is computed by integrating the  $\alpha$  coefficient calculated by the MC-1 indirect method [see Eq. (2)] from  $\mathcal{E}_1$  to  $\mathcal{E}_2$ , with  $\Delta \mathcal{E}$  being the difference between the magnitude of these two fields and always choosing  $\mathcal{E}_1 = 2.0 \times 10^7$  V/m while varying  $\mathcal{E}_2$  when changing  $\Delta \mathcal{E}$ . Two main features can be seen from Fig. 1(b): (i) For any temperature,  $\Delta T$  is not linear with  $\Delta \mathcal{E}$ , as also observed near 310 K in the  $\text{Ba}(\text{Zr}_{0.2}\text{Ti}_{0.8})\text{O}_3$  material [42] exhibiting relaxor behavior and which is in contrast with, e.g., the cases of the ferroelectric  $\text{Pb}(\text{Zr}_{0.95}\text{Ti}_{0.05})\text{O}_3$ ,  $\text{Pb}(\text{Zr}_{0.4}\text{Ti}_{0.6})\text{O}_3$ ,  $(\text{Ba}_{0.5}\text{Sr}_{0.5})\text{TiO}_3$ , and  $\text{Pb}(\text{Mg},\text{Nb})\text{O}_3$ - $\text{PbTiO}_3$  systems reported in Refs. [4, 14, 15, 65]; and (ii) for any given electric field above  $\simeq 1.5 \times 10^8$  V/m,  $\Delta T$  is enhanced when the considered initial temperature increases. Item (i) originates from the fact that  $\alpha$  strongly depends on the electric field and can even be nonmonotonic with  $\mathcal{E}$  in relaxor ferroelectrics (see Fig. 2). Item (ii) can be simply understood by realizing that Eq. (9) provides a dependence of the EC coefficient on temperature. Note that we also numerically checked that our  $\Delta T$ 's are not directly proportional to the power  $2/3$  of the electric field, except for fields above  $10^8$  V/m at 500 K, which contrasts with the prediction of Ref. [23]. Furthermore, our MD predictions for  $\Delta T$  at 100 K are also given for comparison in Fig. 1(b), which demonstrates, once again, that results from direct and indirect approaches differ below  $T_m$ . One should also recall that atomic schemes, such as effective Hamiltonians, typically provide an overestimation by one order of magnitude with respect to experiments for electric fields [66] while they tend to yield correct values for the EC coefficient (as shown in the Supplemental Material). Experiments are thus called for to determine by which factors the temperatures and fields of Fig. 1(b) would have to be rescaled in BZT (if any).

#### IV. SUMMARY

In summary, we combined an atomistic effective Hamiltonian scheme with Monte Carlo and molecular dynamics techniques to investigate the electrocaloric effects in lead-free BZT systems subject to electric fields of different magnitudes and all oriented along the pseudocubic [001] direction. It is

found that, for any temperature,  $\alpha$  exhibits a nonmonotonic behavior with field that consists of small values at low fields, followed by an increase up to a maximum before decreasing for larger fields. Below the Burns temperature, this maximum of  $\alpha$  is demonstrated to be correlated to a very specific microscopic feature, namely, to the largest number of dipoles being oriented along (111) directions having a positive  $z$  component. Finally, equalities that are derived from a simple Landau model (including one relating  $\alpha$  with the product of temperature and the partial derivative of the square of polarization) reproduce and further help to understand the anomalous behavior of  $\alpha$  with field and temperature in BZT, for any temperature above  $T_m$  (note that we also found that this model can predict EC effects in typical ferroelectrics, such as  $\text{BaTiO}_3$ , as shown in the Supplemental Material). Our simulations also confirm that indirect and direct approaches yield similar results of the  $\alpha$  EC coefficient for any temperature above the  $T_m$  temperature but differ from each other for temperature below  $T_m$ , because of the nonergodicity adopted by BZT at these low temperatures [7, 25].

We therefore hope that our study leads to a broader knowledge of EC effects and relaxor ferroelectrics.

#### ACKNOWLEDGMENTS

Z.J., S. Prokhorenko, and L.B. are grateful for DARPA Grant No. HR0011-15-2-0038 (MATRIX program) for support. Z.J. also acknowledges support from the National Natural Science Foundation of China (NSFC), Grants No. 11574246, No. 51390472, and No. U1537210, National Basic Research Program of China, Grant No. 2015CB654903, and China Scholarship Council (CSC No. 201506280055). S. Prosandeev is supported by ONR Grant No. N00014-12-1-1034, and Grants No. 3.1649.2017/4.6 from RMES (Russian Ministry of Education and Science), and No. 16-52-0072 Bel\_a from RFBR (Russian Foundation for Basic Research). Y.N. is supported by ARO Grant No. W911NF-16-1-0227. We also acknowledge funding from the Luxembourg National Research Fund through the intermobility (Grant No. 15/9890527 Greenox, J.Í. and L.B.) and Pearl (Grant No. P12/4853155 Cofermat, J.Í. and E.D.) programs. Some computations were also made possible owing to MRI Grant No. 0722625 from NSF, ONR Grant No. N00014-15-1-2881 (DURIP), and a Challenge grant from the Department of Defense.

Z.J. and S. Prokhorenko contributed equally to this work.

- 
- [1] M. E. Lines and A. M. Glass, *Principles and Applications of Ferroelectrics and Related Materials* (Oxford University Press, New York, 1977).
- [2] F. Jona and G. Shirane, *Ferroelectric Crystals* (Dover, New York, 1993).
- [3] J. F. Scott, *Annu. Rev. Mater. Sci.* **41**, 229 (2011).
- [4] A. S. Mischenko, Q. Zhang, J. F. Scott, R. W. Whatmore, and N. D. Mathur, *Science* **311**, 1270 (2006).
- [5] A. S. Mischenko, Q. Zhang, R. W. Whatmore, J. F. Scott, and N. D. Mathur, *Appl. Phys. Lett.* **89**, 242912 (2006).
- [6] Z. Kutnjak, B. Rožič, and R. Pirc, *Electrocaloric Effect: Theory, Measurements, and Applications*, Wiley Encyclopedia of Electrical and Electronics Engineering (Wiley, Hoboken, NJ, 2015).
- [7] *Electrocaloric Materials*, edited by T. Correia and Q. Zhang (Springer, Berlin, 2014).
- [8] Y. Bai, G.-P. Zheng, and S.-Q. Shi, *J. Appl. Phys.* **108**, 104102 (2010).
- [9] X. Moya, S. K. Narayan, and N. D. Mathur, *Nat. Mater.* **13**, 439 (2014).
- [10] X. Q. Liu, T. T. Chen, Y. J. Wu, and X. M. Chen, *J. Am. Ceram. Soc.* **96**, 1021 (2013).
- [11] Y. Liu, I. C. Infante, X. Lou, D. C. Lupascu, and B. Dkhil, *Appl. Phys. Lett.* **104**, 012907 (2014).

- [12] M. Sanlialp, V. V. Shvartsman, M. Acosta, B. Dkhil, and D. C. Lupascu, *Appl. Phys. Lett.* **106**, 062901 (2015).
- [13] K. Uchino, *Ferroelectric Devices* (Dekker, New York, 2000), Chap. 6.
- [14] S. Prosandeev, I. Ponomareva, and L. Bellaiche, *Phys. Rev. B* **78**, 052103 (2008).
- [15] S. Lisenkov and I. Ponomareva, *Phys. Rev. B* **80**, 140102 (2009).
- [16] I. Ponomareva and S. Lisenkov, *Phys. Rev. Lett.* **108**, 167604 (2012).
- [17] M. C. Rose and R. E. Cohen, *Phys. Rev. Lett.* **109**, 187604 (2012).
- [18] M. Marathe, A. Grünebohm, T. Nishimatsu, P. Entel, and C. Ederer, *Phys. Rev. B* **93**, 054110 (2016).
- [19] W. Geng, Y. Liu, X. Meng, L. Bellaiche, J. F. Scott, B. Dkhil, and A. Jiang, *Adv. Mater.* **27**, 3165 (2015).
- [20] E. Defay, S. Crossley, S. Kar-Narayan, X. Moya, and N. D. Mathur, *Adv. Mater.* **25**, 3337 (2013).
- [21] Y. Liu, B. Dkhil, and E. Defay, *ACS Energy Lett.* **1**, 521 (2016).
- [22] Y. Liu, H. Stroyk, B. Dkhil, and E. Defay, *Appl. Phys. Lett.* **109**, 212902 (2016).
- [23] G. G. Guzmán-Verri and P. B. Littlewood, *APL Mater.* **4**, 064106 (2016).
- [24] M. Marathe and C. Ederer, *Appl. Phys. Lett.* **104**, 212902 (2014).
- [25] S. G. Lu, B. Rožič, Q. M. Zhang, Z. Kutnjak, R. Pirc, M. Lin, X. Li, and L. Gorný, *Appl. Phys. Lett.* **97**, 202901 (2010).
- [26] R. Pirc, Z. Kutnjak, R. Blinc, and Q. M. Zhang, *J. Appl. Phys.* **110**, 074113 (2011).
- [27] B. Rožič, M. Kosec, H. Uršič, J. Holc, B. Malič, Q. M. Zhang, R. Blinc, R. Pirc, and Z. Kutnjak, *J. Appl. Phys.* **110**, 064118 (2011).
- [28] L. E. Cross, *Ferroelectrics* **151**, 305 (1994).
- [29] G. Burns and F. H. Dacol, *Phys. Rev. B* **28**, 2527 (1983).
- [30] H. Vogel, *Phys. Z.* **22**, 645 (1921).
- [31] G. S. Fulcher, *J. Am. Ceram. Soc.* **8**, 339 (1925).
- [32] I.-K. Jeong, T. W. Darling, J. K. Lee, Th. Proffen, R. H. Heffner, J. S. Park, K. S. Hong, W. Dmowski, and T. Egami, *Phys. Rev. Lett.* **94**, 147602 (2005).
- [33] B. Dkhil, P. Gemeiner, A. Al-Barakaty, L. Bellaiche, E. Dul'kin, E. Mojaev, and M. Roth, *Phys. Rev. B* **80**, 064103 (2009).
- [34] O. Svitelskiy, D. La-Orautapong, J. Toulouse, W. Chen, and Z.-G. Ye, *Phys. Rev. B* **72**, 172106 (2005).
- [35] A. R. Akbarzadeh, S. Prosandeev, E. J. Walter, A. Al-Barakaty, and L. Bellaiche, *Phys. Rev. Lett.* **108**, 257601 (2012).
- [36] C. Kittel, *Introduction to Solid State Physics* (Wiley, New York, 2004).
- [37] T. Maiti, R. Gu, and A. S. Bhalla, *J. Am. Ceram. Soc.* **91**, 1769 (2008).
- [38] R. Farhi, M. El Marssi, A. Simon, and J. Ravez, *Eur. Phys. J. B* **9**, 599 (1999).
- [39] A. A. Bokov and Z.-G. Ye, *J. Mater. Sci.* **41**, 31 (2006).
- [40] A. Al-Barakaty, S. Prosandeev, D. Wang, B. Dkhil, and L. Bellaiche, *Phys. Rev. B* **91**, 214117 (2015).
- [41] S. Prosandeev, D. Wang, A. R. Akbarzadeh, B. Dkhil, and L. Bellaiche, *Phys. Rev. Lett.* **110**, 207601 (2013).
- [42] X.-S. Qian, H.-J. Ye, Y.-T. Zhang, H. Gu, X. Li, C. A. Randall, and Q. M. Zhang, *Adv. Funct. Mater.* **24**, 1300 (2014).
- [43] H.-J. Ye, X.-S. Qian, D.-Y. Jeong, S. Zhang, Y. Zhou, W.-Z. Shao, L. Zhen, and Q. M. Zhang, *Appl. Phys. Lett.* **105**, 152908 (2014).
- [44] S. Prosandeev, D. Wang, and L. Bellaiche, *Phys. Rev. Lett.* **111**, 247602 (2013).
- [45] D. Wang, J. Hlinka, A. A. Bokov, Z.-G. Ye, P. Ondrejčević, J. Petzelt, and L. Bellaiche, *Nat. Commun.* **5**, 5100 (2014).
- [46] D. Wang, A. A. Bokov, Z.-G. Ye, J. Hlinka, and L. Bellaiche, *Nat. Commun.* **7**, 11014 (2016).
- [47] W. Zhong, D. Vanderbilt, and K. M. Rabe, *Phys. Rev. B* **52**, 6301 (1995).
- [48] S. Bin-Omran, I. A. Kornev, and L. Bellaiche, *Phys. Rev. B* **93**, 014104 (2016).
- [49] W. G. Hoover, A. J. C. Ladd, and B. Moran, *Phys. Rev. Lett.* **48**, 1818 (1982).
- [50] D. J. Evans, *J. Chem. Phys.* **78**, 3297 (1983).
- [51] I. P. Omelyan, I. M. Mryglod, and R. Folk, *Comput. Phys. Commun.* **151**, 272 (2003).
- [52] Note that the molecular dynamics simulations conducted here were done without a full account of strain dynamics following the approach of Ref. [18]. As a result, the results for the EC coefficient for the MD method were renormalized (multiplied by a factor of  $C'_\epsilon/C_\epsilon$ , where  $C'_\epsilon$  corresponds to specific heat computed from MD simulations using fluctuation-dissipation theorem), in order to account for the concomitant change in the specific heat. Note, however, that we also performed MD simulations that include strain dynamics for some temperatures and found that the corresponding  $\alpha$  coefficient is very similar (namely, within 2%) to this renormalized one for investigated electric field values.
- [53] S. G. Lu, B. Rožič, Z. Kutnjak, and Q. M. Zhang, *Electrocaloric Effect (ECE) in Ferroelectric Polymer Films, in Ferroelectrics*, edited by I. Coondoo (InTech, Austria, 2010), Chap. 6.
- [54] See Supplemental Material at <http://link.aps.org/supplemental/10.1103/PhysRevB.96.014114> for more details about the EC effects in BaTiO<sub>3</sub> and BZT, which includes Refs. [16,36,55–59].
- [55] L. Walizer, S. Lisenkov, and L. Bellaiche, *Phys. Rev. B* **73**, 144105 (2006).
- [56] C. Ménot, J. M. Kiat, B. Dkhil, M. Dunlop, H. Dammak, and O. Hernandez, *Phys. Rev. B* **65**, 224104 (2002).
- [57] V. V. Lemanov, E. P. Smirnova, P. P. Syrnikov, and E. A. Tarakanov, *Phys. Rev. B* **54**, 3151 (1996).
- [58] A. Karchevskii, *Sov. Phys. Solid State* **3**, 2249 (1962).
- [59] X. Moya, E. Stern-Taulats, S. Crossley, D. González-Alonso, S. Kar-Narayan, A. Planes, L. Mañosa, and N. D. Mathur, *Adv. Mater.* **25**, 1360 (2013).
- [60] F. L. Goupil, A. Berenov, A.-K. Axelsson, M. Valant, and N. M. Alford, *J. Appl. Phys.* **111**, 124109 (2012).
- [61] Y.-B. Ma, A. Grünebohm, K.-C. Meyer, K. Albe, and B.-X. Xu, *Phys. Rev. B* **94**, 094113 (2016).
- [62] Note that the second line of Eq. (9) can also be derived from the equality  $dT = \frac{2A}{C} T P dP$  provided in Ref. [63], where  $A$  is constant and where  $C$  is a specific heat.
- [63] B. A. Strukov, *Sov. Phys. Crystallogr.* **11**, 757 (1967).
- [64] Assuming that  $P = \chi \mathcal{E}$ , where  $\chi$  is the dielectric susceptibility, yields  $\frac{\partial P^2}{\partial \mathcal{E}} \Big|_T = 2\chi^2 \mathcal{E}$ . This latter equality therefore explains why  $\frac{\partial P^2}{\partial \mathcal{E}} \Big|_T$  is small for low electric fields, at any temperature.
- [65] D. Saranya, A. R. Chaudhuri, J. Parui, and S. B. Krupanidhi, *Bull. Mater. Sci.* **32**, 259 (2009).
- [66] B. Xu, J. Íñiguez, and L. Bellaiche, *Nat. Commun.* **8**, 15682 (2017).